


RESEARCH

Open Access



# Remote interference management in 5G new radio: methods and performance

Elena Peralta<sup>1\*</sup> , Toni Levanen<sup>1</sup>, Mikko Mäenpää<sup>3</sup>, Youngsoo Yuk<sup>4</sup>, Klaus Pedersen<sup>5</sup>, Sari Nielsen<sup>2</sup> and Mikko Valkama<sup>6</sup>

\*Correspondence:  
elena.peralta\_calvo@nokia.com

<sup>1</sup> Nokia Bell Labs, Tampere, Finland

Full list of author information is available at the end of the article

## Abstract

In time division duplexing based mobile networks, under certain atmospheric ducting conditions, the uplink reception may be interfered by the downlink transmissions of remote base-stations (gNBs) located hundreds of kilometers away. This paper addresses such remote interference problem in a 5G new radio (NR) macro deployment context. Specifically, two potential reference signal (RS) designs for remote interference management (RIM) are described. The first signal structure, denoted as the one OFDM symbol (1OS) based RIM-RS, is building on the channel state information reference signals of 5G NR. The second candidate is referred to as the two OFDM symbol based RIM-RS design, which builds on the design principles of LTE RIM-RS. The achievable detection performance is evaluated by introducing enhanced receiver algorithms together with three feasible propagation delay based gNB grouping and corresponding RIM-RS transmissions schemes. The performance results in terms of the receiver processing gain highlight that the improved detection algorithm assures sufficient performance to detect the remote interference for both RIM-RSs with all evaluated frequency domain comb-like patterns. The benefit of grouping corresponding RIM-RS transmissions from gNBs located on the same area is greater when using same frequency domain resources per transmitted sequence in practical interference scenarios. Furthermore, applying a common base sequence for all gNBs within a group allows to identify the group based on detected sequence and enables adaptive RIM mitigation schemes. On the other hand, it is shown that the 1OS RIM-RS provides smaller overhead and can be frequency multiplexed with the physical downlink shared channel, which opens up the possibility of using gNB group wise 1OS RIM-RS also for UE interference measurements.

**Keywords:** Remote interference management, 5G new radio (NR), Atmospheric ducting, Physical layer design

## 1 Introduction

### 1.1 Background and basics

The large number of base stations envisioned for the dense deployment of the fifth generation new radio (5G NR) mobile networks [1, 2] motivates the development of efficient remote interference management (RIM) schemes. The remote interference appears even for the case of fully synchronized time division duplexing (TDD) networks, due to propagation time differences and ducting phenomenon, where all gNBs are using the

same radio frame configuration. The so-called atmospheric ducting phenomena can impact the signal-to-interference-and-noise ratio in the uplink (UL) reception of a 5G NR base station (called gNB) by the downlink (DL) transmissions from a remote gNB. In particular, the ducting phenomena takes place when the radio waves propagate within a duct of warm air in the troposphere [3] due to specific temperature and humidity conditions [4–6]. In the event of atmospheric ducting, the radio waves experience a bending effect propagating within the ducting boundaries even for hundreds of kilometers [7], as illustrated in the upper part of Fig. 1.

In general, there are experimental studies in the literature addressing and analysing the effects of the ducting while establishing, e.g., corresponding pathloss and fading models. In [3, 8], atmospheric duct channel models are proposed, in the context of terrestrial and maritime communications, establishing statistical large-scale path-loss models for surface ducts based on parabolic equations to predict the distribution of small-scale fading. It is concluded that the fading in the channel follows a Rayleigh fading model. In [8], it is observed that an increase of 1 degree on the antenna downtilt can decrease the RI power by 2 to 3 dB while it is also shown that depending on the distance between aggressor and victim gNBs, the RI can be stronger for different antenna heights. Additionally, in [9], an increased RI level in Korea’s LTE-TDD system was shown due to Japan’s WiMax gNB from a distance of 240km, especially in cell radius of 0.5 km compared to smaller cells. In this practical study, it was observed that the path loss between both gNBs is about 142 dB when the height of both antennas is 30 meters—a path loss value lower than the free space propagation loss with the same distance.

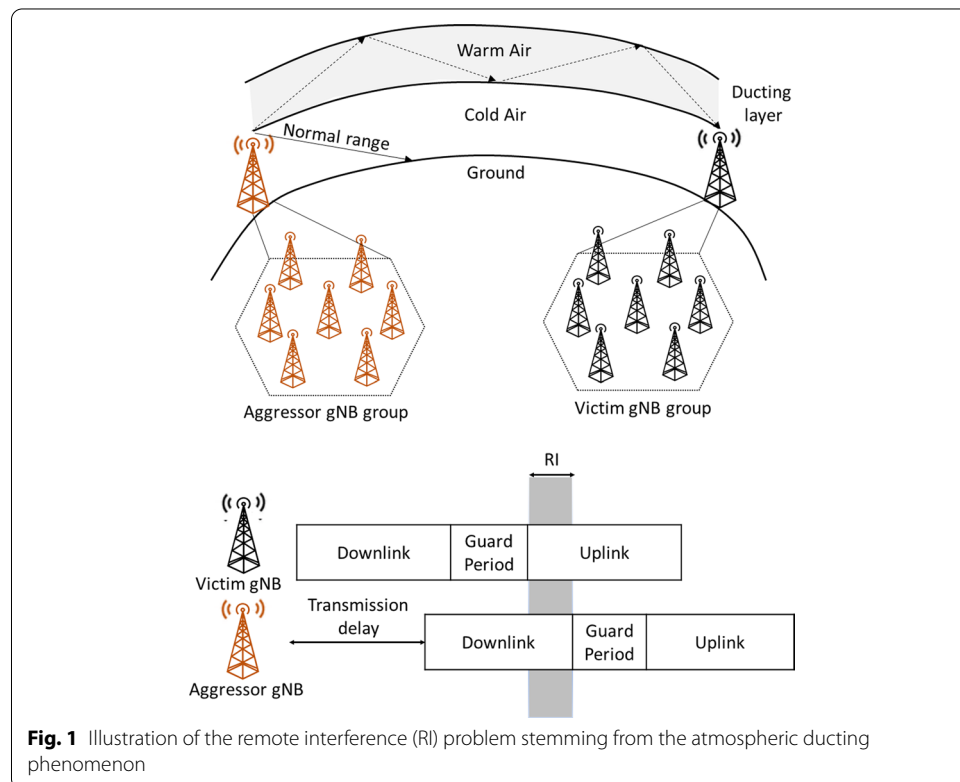


**Fig. 1** Illustration of the remote interference (RI) problem stemming from the atmospheric ducting phenomenon

## 1.2 RIM and 5G NR

The remote interference problem stemming from the atmospheric ducting phenomena has been recently investigated in 3GPP 5G NR technical reports, see e.g. [10]. There the overall aim was to investigate possible mitigation schemes to improve the network robustness against remote gNB interference, focusing primarily on TDD macro cells with semi-static DL/UL configurations. To this end, the guard period (GP) between DL and UL transmissions can already be increased in TDD-based long term evolution (TD-LTE) networks if an aggressor gNB can be detected and identified [11]. In general, the longer is the distance to the aggressor gNB, the higher is the number of UL symbols impacted at the victim gNB as illustrated conceptually in the bottom part of Fig. 1. As a concrete example, assuming subcarrier spacing (SCS) of 15 kHz mapping to a symbol duration of 66.7  $\mu$ s, and cyclic prefix (CP) of 4.7  $\mu$ s, and considering 100 km distance between the aggressor and the victim gNBs, the propagation delay corresponds to approximately five OFDM symbols. Relying on synchronized TDD macro cells to divide UL and DL radio resources, the impact of this ducting phenomena is expected to be even higher in 5G NR networks when deploying larger number of base stations compared to TD-LTE scenarios [10]. Hence, efficient mechanisms for remote interference management in NR (NR-RIM) should be investigated due to the large amount of possible interference sources with different propagation delays.

The fundamental task of NR-RIM is to detect when the remote interference occurs, to identify the group of interfering gNBs, and finally to measure the propagation delays between the aggressor and victim gNB or groups of gNBs. To this end, two potential RIM reference signal (RIM-RS) designs were presented in a previous study [12] and evaluated in terms of remote interference detection probability together with the receiver processing framework. The so-called one OFDM symbol (1OS) RIM-RS design is proposed based on the 5G NR channel state information reference signal (CSI-RS), while the two OFDM symbol (2OS) RIM-RS design is built similar to the LTE RIM-RS. The preliminary findings in [12] show the suitability of the 1OS RIM-RS when increasing the number of gNBs transmitting different RIM-RS sequences, due to the shorter time duration of this design and the reduced probability for overlapping between sequences in the receiver, compared to the 2OS case. Specifically, both RIM-RS structures were evaluated in the study in [12] to verify the achievable performance with increased number of transmitting gNBs. Also, it was assumed that a pool of different RIM-RS sequences were transmitted from different gNBs within a given propagation delay range and using the same frequency domain resources based on the 3GPP agreements [10].

## 1.3 Contributions and novelty

This article comprehensively extends the preliminary work and results in [12] in terms of detection performance analysis in the RIM framework investigating possible propagation delay based gNB grouping and corresponding RIM-RS transmission schemes. It is assumed that the network operator would group gNBs on a specific region to simultaneously transmit RIM-RSs, as the atmospheric ducting phenomenon is typically affecting relatively large regions simultaneously. In the proposed approach, enhanced transmission schemes are analyzed to evaluate the achievable performance gain when using the same frequency domain resources to transmit all RIM-RS sequences or when using

frequency-division multiplexing to transmit either the same or, different base sequences within a gNB group. In addition, we evaluate the achievable performance gain for both RIM-RS designs by introducing enhanced receiver algorithms with increased number of detection windows. The moderate increase in the detection complexity is alleviated by the low periodicity of the RIM-RS and justified by the observed performance gains. The obtained results indicate that the improved receiver processing algorithm assures that both RIM-RS designs, 1OS and 2OS, can provide sufficient performance to detect the remote interference under the atmospheric ducting phenomenon. In RIM scenarios where large number of gNBs are deployed, propagation delay based gNB grouping and using the same frequency resources for all RIM-RSs is shown to lead to the best detection performance. The presented methods and results provide novel findings for the first practical RIM deployment scenarios in the presence of large number of gNBs, which are not available in earlier studies in the related literature.

The rest of the paper is organized as follows: Sect. 2 describes the NR-RIM framework at high level, the two RIM-RS designs used to detect the remote inter-gNB interference and, the three propagation delay based gNB grouping schemes proposed to transmit the RIM-RS sequences from multiple gNBs in 5G NR networks. Then, in Sect. 3, the detection algorithm and considered performance metrics are described. In Sect. 4, the detection performance of the proposed schemes and new detection methodology are evaluated and analyzed. Finally, Sect. 5 concludes the paper.

## 2 Methods for RIM in 5G NR

### 2.1 High level NR-RIM framework

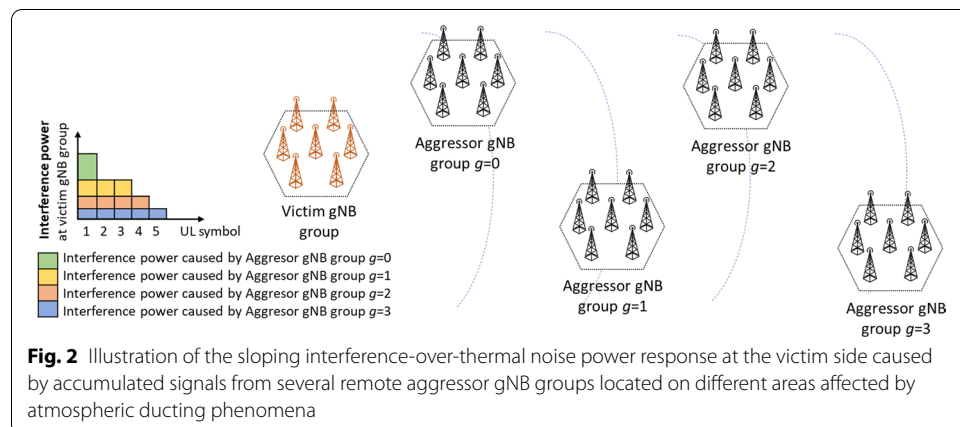
In TD-LTE networks, the RIM framework relies on manual intervention through OAM (operations, administration and maintenance) to monitor and start or stop transmitting the RIM-RS. There is therefore significant room for improvement in order to minimize the manual intervention in the event of ducting phenomena and to increase the network performance and efficiency. Depending on the network configuration, a group of aggressor or victim gNBs, located in the same area where atmospheric ducting phenomenon occurs, may transmit the RIM-RS sequence within the same transmission period and same ID group. Due to channel reciprocity, the interference can be measured in the victim or aggressor side. In this context, the first 3GPP specifications for NR-RIM [10] assume that the whole network with synchronized macro cells has a common understanding on the DL and UL transmission and reception boundaries.

Based on the study of different mechanisms [10], static and adaptive RIM schemes can be considered in 5G NR. Static RIM schemes rely on network planning, i.e., configuring large guard periods to cover long propagation delays that could provide robustness against the ducting phenomenon. Besides, dynamic TDD configurations can be applied when the RI takes place, such as UL or DL muting at victim or aggressor side, respectively, as well as using orthogonal frequency multiplexed resources between victim UL and aggressor DL. However, there is a trade-off between these RI mitigation schemes and the achievable throughput performance. On the other hand, placing antennas at lower height, or correcting the antenna tilt to reduce the interference power, may be applied at victim side at cost of network coverage and average performance. Aiming to increase the network efficiency, adaptive schemes can be applied only in the event of

remote interference, such as the use of beamforming to attenuate received signal at the victim side in the direction of the remote interference. For instance, in [13], it is proposed to perform a beam nulling operation in the direction of the RI or in [14], it is shown that the tropospheric ducting interference tend to be highly directional so the interference level can be 10 to 30 dB higher at the antennas pointing towards the RI source compared to the antennas pointing to other directions. Nevertheless, it should be noted that although enhanced digital beamforming techniques can be expected to alleviate the remote interference problem to certain extent, they cannot completely remove it.

The adaptive schemes require coordination between victim and aggressor gNBs to be enabled. In the first NR-RIM framework, a set of victim gNBs located in an area affected by atmospheric ducting, experience the so-called interference-over-thermal-noise power response [10], illustrated in Fig. 2, and start RIM-RS-A transmissions using the same RIM-RS and ID set. In particular, the sloping interference power response over different UL OFDM symbols is caused by accumulated signals from several remote aggressor gNBs or groups of gNBs with different distances. The RIM-RS-A signal allows the aggressor gNBs to recognize the event of ducting and determine how many UL resources are affected at the victim side. Upon reception of the RIM-RS-A, aggressor gNBs apply RIM mitigation schemes, such as muting necessary DL resources, and start to transmit RIM-RS-B signal to assist the victim side to decide whether the ducting phenomena still remains. Victim gNBs continue monitoring the detection of RIM-RS-B and may stop RIM-RS-A transmissions if RIM-RS-B is not detected and the sloping interference power response goes down to normal levels. It should be noted that both RIM-RS-A and RIM-RS-B carry different functionalities but should follow the same design principles [10]. On the other hand, a second feasible NR-RIM framework can follow the same workflow as described above, but the victim gNB set is informed of the reception of the RIM-RS-A by the group of aggressor gNBs through the backhaul after applying the corresponding mitigation scheme.

These potential RIM-RS frameworks and possible RIM backhaul-based signalling via the 5G core network have been discussed in [10]. An example of a conceptual NR-RIM framework is illustrated in Fig. 2 as captured in 3GPP agreements [10]. In this context, this paper focuses on possible propagation delay based gNB grouping transmissions, where gNBs located on the same area may simultaneously transmit the same RIM-RS



sequence allowing to differentiate them from other aggressor gNB groups based on detected time delay or RIM-RS sequence.

## 2.2 NR-RIM reference signal designs

Two alternative RIM-RS designs are analyzed as exhibited in a previous study [12], following the RS requirements defined by 3GPP specifications [10]. In TD-LTE networks, the RIM-RS adopts a repetitive structure so that the detection can be done at OFDM symbol level in the receiver. Symbol level detection is considered also in 5G NR RIM studies to reduce the detector complexity in the gNB.

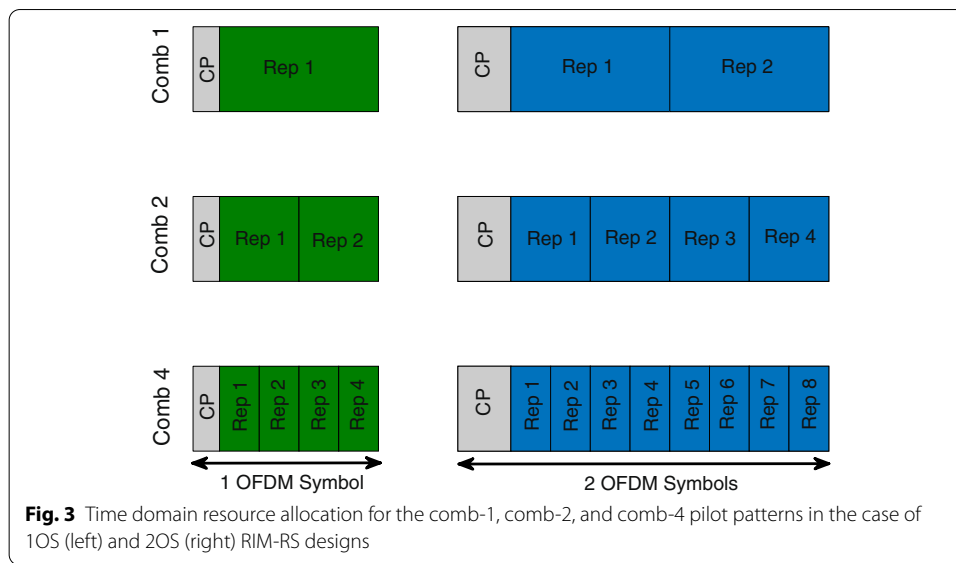
### 2.2.1 1OS RIM-RS

The existing NR reference signals support flexible configuration and could thus be considered as the starting point also for RIM-RS design. Considering the available synchronization signals for the remote interference detection, e.g., primary and secondary synchronization signals (PSS and SSS), we note that they may not be transparent to a user equipment (UE) trying to perform initial access procedures and, therefore, they are not considered for NR-RIM. The demodulation reference signal (DM-RS) is optimized for channel estimation in synchronized operation and it is never transmitted in the last DL symbol of a slot in 5G NR Release-15 [15], therefore, it is not considered in the NR RIM-RS development. On the other hand, especially when considering the backward compatibility, the NR CSI-RS which is defined only for DL can be mapped to any OFDM symbol within a slot and can be signaled to be transparent to a UE. The CSI-RS design also allows several resource allocation densities and may contain a repetitive structure in the time domain within one OFDM symbol due to the comb-like mapping to the frequency domain resources [15].

The 1OS RIM-RS design, which builds on the 5G NR CSI-RS, supports a repetition structure in the time domain within one OFDM symbol [15]. The so-called comb-like mapping can be directly adopted in frequency domain for RIM-RS designs, where the RS is transmitted in every  $N_{\text{rep}}^{\text{th}}$  subcarrier, which corresponds to a  $N_{\text{rep}}$  wise repetition structure in the time domain within one OFDM symbol [12]. In 5G NR Release-15, the CSI-RS supports a comb-type mapping where the signal is allocated in every fourth subcarrier in the frequency domain (referred to as comb-4), which is then observed as 4-times repetitive structure in the time domain within one OFDM symbol, as illustrated in Fig. 3. The signal does not directly supports comb-1 and comb-2 structures, but preliminary results [12] showed that by enabling 3 dB and 6 dB power boosting for comb-2 and comb-4 patterns, respectively, similar detection performance can be achieved for all comb-patterns with a single sequence transmission from one gNB. In this case, the CSI-RS power boosting sets the relative power boosting (in dB) of the CSI-RS associated with the physical downlink shared channel (PDSCH) relative to the PDSCH power. Hence, the RIM-RS is transmitted without the physical downlink shared channel carrying user data.

### 2.2.2 2OS RIM-RS

In TD-LTE networks, the RIM-RS adopts a repetitive structure similar to the physical random access channel (PRACH) preamble formats 2 and 3 [16]. The main difference



between the RIM-RS and UL PRACH preamble designs is that the RIM-RS is assumed to occupy the full allocation bandwidth. The 2OS RIM-RS design, similar to the LTE RIM-RS, builds on two identical copies of the selected full-band PRACH sequence while the CP length is doubled to align the number of transmitted samples with two CP-OFDM symbols. Similar to the 1OS design, three comb-like mappings have been adopted in frequency domain for the 2OS RIM-RS. In addition, it was observed that all cyclic shifts (CSs), i.e. cyclically shifting the comb-pattern in frequency domain, result in the same detection performance. Therefore, both RIM-RS designs, 1OS and 2OS, support two CSs for comb-2 and four CSs for comb-4, respectively, as shown in Fig. 3.

These RIM-RS structures are primarily designed to maximize the detection performance in the NR-RIM framework. However, the 1OS RIM-RS design could also be used to perform channel interference measurements on neighbouring UEs located on the same area. To achieve this, new transmission schemes can be deployed to group gNBs located on a specific area affected by ducting based on the knowledge of the RIM-RS sequences transmitted and resources allocated. Therefore, the RIM-RS resources from neighbour gNBs can be interpreted as scheduled non-zero power CSI-RS resources (NZP CSI-RS) or zero power CSI-RS (ZP CSI-RS). In this context, the 2OS RIM-RS design cannot be used for interference measurements as it breaks the symbol alignment of the 5G NR physical layer.

### 2.2.3 Sequence generation

The achievable performance in terms of the detection, false alarm, and detection error probabilities for both RIM-RS designs depends on the auto- and cross-correlation properties of the adopted sequences. Pseudo-random sequences generated from a length-31 Gold sequence are widely used in 5G NR [15, 17]. They provide good detection performance due to the good auto- and cross-correlation properties and, hence, were assumed as baseline for RIM studies [10]. In this study, a maximum number of eight different initialization values are assumed [12], which correspond to eight different base sequences

to be detected. The base sequences were chosen so that their cross-correlation coefficients are below 0.1. The actual complex RIM-RS sequence,  $\mathbf{r}_n$ , is QPSK modulated and defined for each base sequence  $n$  as

$$r_n(s) = \frac{1}{\sqrt{2}}[(1 - 2c_n(2s)) + j(1 - 2c_n(2s + 1))], \quad (1)$$

where  $s \in \{0, 1, \dots, S - 1\}$ , and the pseudo-random sequence  $\mathbf{c}_n$  is defined in [15, Section 5.2.1], for the eight given initialization values in [12], leading to the eight possible base sequences. Considering the frequency domain comb-1, comb-2, and comb-4 RS patterns, three different sequence lengths  $S = 600$ ,  $S = 300$  or  $S = 150$  are evaluated, respectively. Additional details on the selected sequences can be found from [12].

### 2.3 Considered NR-RIM transmission schemes

Following 3GPP guidelines as captured in [10], we verified in a previous study [12], the achievable detection performance for both RIM-RS designs in simple scenarios, corresponding to the cases C1, C2 and C3 in Table 1. In this study, we focus our evaluations on the most challenging and practical scenario, case C4, for which preliminary detection performance results for a large number of gNBs transmitting simultaneously several copies of different base sequences were depicted in [12]. For all the given evaluations in [12], the RIM-RS sequences transmitted from different gNBs were uniformly distributed within the expected propagation delay range.

It is, however, expected that the number of gNBs deployed per operator and located in different areas affected by ducting phenomenon will be considerably larger for practical NR-RIM scenarios. Thus, to address this problem, this work concentrates on enhanced transmission schemes to group gNBs located on a specific area to simultaneously transmit RIM-RS sequences. As illustrated in Fig. 2, the aggressor gNB group  $g = 1$ , may transmit the RIM-RS at different DL transmission time than the DL transmission time of a gNB located on another area, i.e, aggressor gNB group  $g = 2$ , with the possibility of using different RIM-RS sequence per gNB group to differentiate them either based on detected delay or base sequence. The detection based on propagation delay requires that in the network level there is information of the relative distances between different gNB groups. We assume that the aggressor groups have uniformly distributed distances to the victim gNB group, each group is comprised of  $M_G = 10$  gNBs, and that the arrival time of transmissions from gNBs within the same group can be any value within the cyclic prefix duration. The main parameters used throughout this paper are summarized in Table 2 for notational clarity.

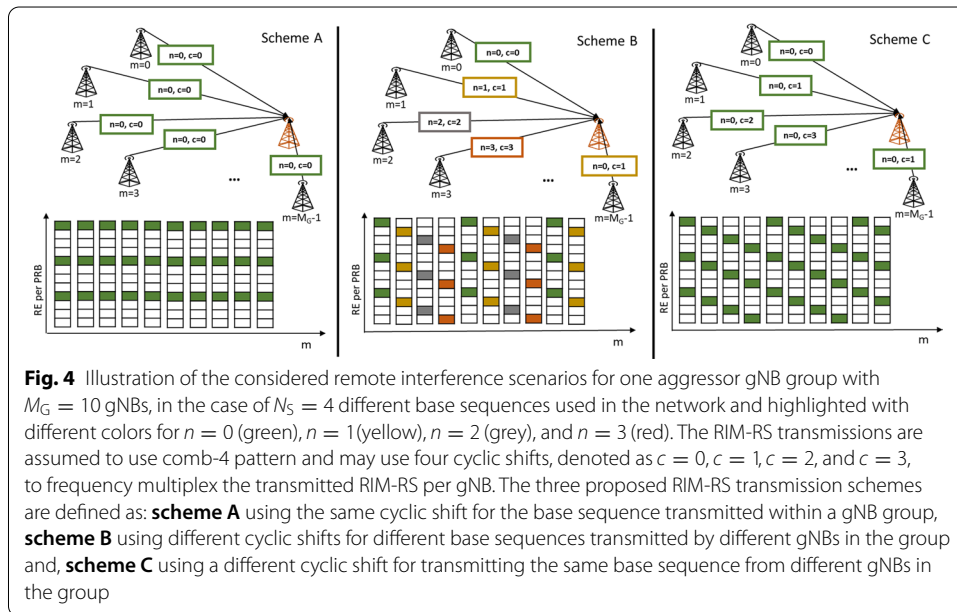
**Table 1** 5G NR RIM evaluation cases

Case description	$N_S$	$M_C$
C1	Single copy of a single sequence	1
C2	Multiple copies of a single sequence	10
C3	Single copy of multiple sequences	{1, 2, 4, 8}
C4	Multiple copies of multiple sequences	{1, 2, 4, 8}



**Table 2 Main parameters and their definitions used throughout this paper**

Parameter	Definition
$N_S \in \{1, 2, 4, 8\}$	Number of different base sequences used in the network. In this work, the maximum number of different base sequences is limited to eight
$n \in \{0, 1, \dots, N_S - 1\}$	Base sequence index
$M_C \in \{10, 20, 40, 80\}$	Number of gNBs transmitting a copy of the same base sequence
$M_{gNB} = N_S M_C$	Total number of gNBs transmitting a RIM-RS and the number of sequences arriving to the receiver within a delay window
$M_G = 10$	Number of gNBs per group. In this work, a constant value of 10 is assumed
$m \in \{0, 1, \dots, M_G - 1\}$	gNB index within a gNB group
$G = M_{gNB}/M_G$	Number of aggressor gNB groups
$g \in \{0, 1, \dots, G - 1\}$	Aggressor gNB group index
$K = 600$	Total number of resource elements (REs) allocated for the base sequence
$k \in \{0, 1, \dots, K - 1\}$	Frequency domain RE index
$S$	Length of the used base sequence
$s \in \{0, 1, \dots, S - 1\}$	Sample index within the used base sequence
$c \in \{0, 1, 2, 3\}$	Cyclic shift index used for transmitting a specific base sequence. Maximum number of cyclic shifts depends on the used frequency domain comb-pattern.
$N_{rep} \in \{1, 2, 4\}$	Number of time domain repetitions with comb-1, comb-2, and comb-4 frequency patterns.



Prior studies [12] were carried out by transmitting all RIM-RS sequences using the same frequency domain resources to provide first detection performance comparison between RIM-RS designs based on 3GPP evaluation assumptions [10]. This scenario corresponds to the so-called Scheme A, as illustrated in Fig. 4. The auto- and cross-correlation properties of the selected sequences dominate the detection performance and separation capability between different sequences. Hence, mapping the RIM-RS sequences from an aggressor or victim gNB group to different frequency resources

could improve the detection performance achieved in NR networks in presence of large amount of interference sources. The aforementioned scenario corresponds to the proposed Scheme C, as illustrated in Fig. 4.

On the other hand, the 1OS RIM-RS design opens up the possibility of performing channel interference measurements on UEs served by the gNBs in the aggressor group, assuming that the UEs can interpret the RIM-RS resources as NZP CSI-RS or ZP CSI-RS resources. Therefore, allocating several base sequences to different frequency resources within the same gNB group, allows UEs to perform RIM-RS based interference measurements based on the knowledge of different base sequences and frequency resources used by the neighbour gNBs. This scenario corresponds to the proposed Scheme B in Fig. 4. As we noticed in Sect. 2.2, the 2OS RIM-RS design cannot be used for interference measurements by the UEs as it breaks the symbol alignment of the 5G NR physical layer. The evaluation of the considered RIM-RS transmission schemes from the UE interference measurement point of view is an interesting future research topic.

The presented schemes facilitate the RIM-RS sequences transmitted from several gNBs within a group to be frequency multiplexed by assigning them with different CSs. The transmission schemes proposed in this study to group RIM-RS sequences transmitted from several gNBs in the NR-RIM framework are illustrated in Fig. 4, when using a comb-4 structure as an example. More specifically, the exact frequency domain resources used for the transmitted sequences are illustrated for one aggressor group comprised of  $M_G = 10$  gNBs.

The frequency domain response of all transmitted RIM-RSs within an area affected by ducting phenomena is defined as  $\alpha^{(g,m)}$  for each aggressor gNB group  $g \in \{0, 1, \dots, G - 1\}$  and gNB  $m \in \{0, 1, \dots, M_G - 1\}$  within the aggressor group. Here,  $G$  is the number of aggressor gNB groups and  $M_G$  is the number of gNBs per aggressor group. The sequence  $\mathbf{r}_n$  is mapped to corresponding RIM-RS,  $\alpha^{(g,m)}$ , according to

$$\alpha^{(g,m)}(k) = \sqrt{N_{\text{rep}}} r_n(s), \tag{2}$$

where  $s \in \{0, 1, \dots, S - 1\}$ ,  $n \in \{0, 1, \dots, N_S - 1\}$  and  $N_S$  is the number of used base sequences,  $k = sN_{\text{rep}} + c$  is the specific frequency resource element to which the signal component is mapped, and  $c \in \{0, 1, 2, 3\}$  is the CS value used for gNB index  $m$  in gNB group index  $g$ . Scaling the pseudorandom sequence  $\mathbf{r}_n$  with the square root of the number of repetitions,  $N_{\text{rep}}$ , normalizes the transmitted signal power to same level with different frequency domain comb patterns.

The exact design principles for each scheme, the used cyclic shift value  $c$ , and the base sequence index  $n$ , can be described and summarized as follows:

*Scheme A)* Following the design assumptions in [10], all RIM-RS sequences are transmitted using the same frequency domain resources and aggressor gNBs are grouped according to the base sequence transmitted. In this case, the used cyclic shift is defined as

$$c = c_A, \tag{3}$$

where  $c_A$  is the network specific cyclic shift value used in all gNB groups. The sequence index used for a specific gNB group is defined as

$$n = \text{mod}(g, N_S). \quad (4)$$

*Scheme B)* The different base sequences are multiplexed in frequency domain using one CS per sequence. For the comb-4 structure, two different CSs are used per base sequence when  $N_S = 2$  base sequences are used in the network, while one CS is used per base sequence when  $N_S = 4$  sequences are used in the network. When  $N_S = 8$  different base sequences are used in the network, two sequences are mapped to the same frequency resources, which could lead to a performance degradation due to the cross correlation properties of two overlapping base sequences. For the comb-2 pattern, the same logic is followed to multiplex the different base sequences. In this scheme, all  $M_C$  copies of the same base sequence are transmitted using the same CS, and the gNB specific CS is defined as

$$c = \text{mod}(m + gM_G, N_{\text{rep}}). \quad (5)$$

The sequence index used for a specific gNB is defined as

$$n = \text{mod}(m + gM_G, N_S). \quad (6)$$

*Scheme C)* Within a gNB group, each copy of the same base sequence is mapped to the frequency domain using a different CS. In this scheme, the gNB specific cyclic shift value is given as

$$c = \text{mod}(m + gM_G, N_{\text{rep}}). \quad (7)$$

The sequence index used for a specific gNB group is defined as

$$n = \text{mod}(g, N_S). \quad (8)$$

### 3 Detection algorithms and performance metrics

#### 3.1 Detection algorithm

The main processing approach for the remote interference detection is to coherently combine the received RIM-RS repetitions within one detection window, after a sequence correlation in the frequency domain against a local replica of the RIM-RS signal, as described in [12]. This process, including correlation peak based weighted averaging of time domain repetitions, is described in Algorithm 1.

A fixed detection threshold for the correlator output was used in [12], based on Chebyshev's inequality [18], for the so-called Detector 1. This detector provides slightly degraded final detection performance due to non-constant false error probability. In this study, we introduce an enhanced receiver algorithm, Detector 2, where we use the information of the distribution of the noise correlation peaks to obtain the proper detection threshold. The distribution is collected from the correlator outputs with inputs containing only noise, obtained when the RIM-RS is not transmitted, to enhance the detection performance and to update the detection threshold based on a given false alarm target as described in Algorithm 2. This allows us to accurately match the targeted false alarm

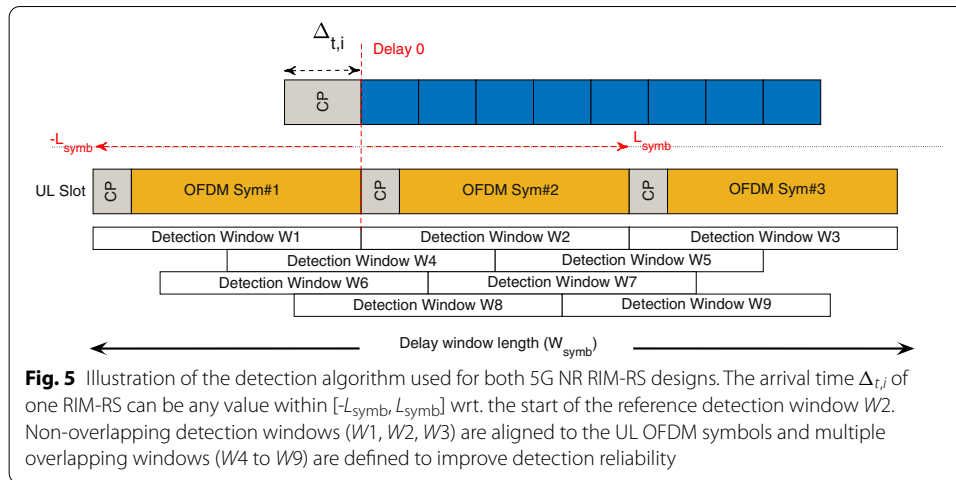


**Table 3 Physical layer parameterization and detection algorithm design**

	Simulation assumptions
Carrier frequency (GHz)	3.5
Bandwith (MHz)	20
Sub-carrier spacing (kHz)	30
Slot duration (ms)	0.5
Channel model	AWGN with random phase rotation or TDL-E
Symbol duration ( $L_{symb}$ )	FFT size + CP length = 1024 + 72
Antenna configuration	1 Tx × 1 Rx
Waveform	CP-OFDM
	<b>Detection algorithm</b>
$N^Q$ detection windows ( $N_w$ )	5, 9 (1OS) or 3, 5 (2OS)
Sequence type	Length-31 Gold Sequence
Frequency pattern	comb-1, -2 or -4
Sequence length (S)	600, 300 or 150
Detection window length	$1 \times L_{symb}$
Delay window length ( $W_{symb}$ )	$3 \times L_{symb}$

probability in all evaluated scenarios. Both algorithms, Detector 1 and Detector 2, are evaluated and compared in the upcoming evaluations for both 5G NR RIM-RS designs. The main physical layer parameters and most essential parameters of the detection algorithm are defined in Table 3.

A high level illustration of the detection windows location and delay window definition is provided in Fig. 5. The detection window length,  $L_{symb}$ , corresponds to one uplink OFDM symbol and for simplicity, we assume that the RIM-RS and UL OFDM symbols have equal lengths. The delay window length,  $W_{symb}$ , corresponds to three OFDM symbols, and it defines the time interval within which the receiver is able to detect the RIM-RS given the propagation delay range of  $[-L_{symb}, L_{symb}]$  [10]. As pointed out in [12], the doubled length of the 2OS RIM-RS provides higher detection probability compared to the 1OS RIM-RS design and, therefore, we noted that at least two ( $W_2, W_3$ ) and three ( $W_1, W_2, W_3$ ) non-overlapping detection windows for the 2OS and 1OS RIM-RS designs, respectively, were required to detect any RS arriving within the delay window  $W_{symb}$ . To

improve detection performance in [12], the number of used detection windows is set to three and five for 2OS and 1OS RIM-RS designs, respectively. These values are assumed as a baseline in this study.

We evaluate the achievable performance gain obtained for both RIM-RS designs by introducing additional detection windows when using the enhanced detector, Detector 2. For the 1OS RIM-RS, the detection performance is analyzed when introducing four additional overlapping windows ( $W_6, W_7, W_8, W_9$ ) delayed 1/4 and 3/4 times  $L_{\text{Symb}}$ , with respect to the first detection window  $W_1$ , as illustrated in Fig. 5. For the 2OS RIM-RS design, we analyze the detection performance including two additional windows ( $W_4, W_5$ ). Due to the low periodicity of the RIM-RS, five and nine detection windows for the 2OS and 1OS RIM-RS designs, respectively, can improve the detection reliability without significantly increasing the overall detection complexity. Further increasing the number of detection windows does not provide any significant gain.

---

**Algorithm 1** Detection algorithm
 

---

```

1:  $N_{\text{slots}} = 0$  ▷ Number of received slots
2:  $\mathbf{y}_{j,k}$  ▷ Received RIM-RS samples
3:  $N_{\text{RS}} = 0$  ▷ Number of slots with allocated RIM-RS
4: for  $s = 1$  to  $N_{\text{slots}}$  do ▷ Loop over slots
5:   for  $n = 1$  to  $N_s$  do ▷ Loop over base sequences
6:     for  $j = 1$  to  $N_w$  do ▷ Loop over detection windows
7:       for  $k = 1$  to  $N_{\text{rep}}$  do ▷ Loop over time repetitions
8:          $\mathbf{b}_{n,j,k} = \mathcal{F}^{-1} \{ \mathbf{r}_n^* \cdot \mathcal{F} \{ \mathbf{y}_{j,k} \} \}$  ▷ Correlation
9:          $x_{n,j,k} = \max(|\mathbf{b}_{n,j,k}|^2)$ 
10:       end for
11:        $t_k = x_{n,j,k} / \sum_{k=1}^{N_{\text{rep}}} x_{n,j,k}$  ▷ Peak based weighting
12:        $\mathbf{o}_{n,j} = \sum_{k=1}^{N_{\text{rep}}} t_k \mathbf{b}_{n,j,k}$ 
13:        $\mathbf{o}_n = \text{concatenate}(\mathbf{o}_n, \mathbf{o}_{n,j})$ 
14:     end for
15:      $p(n) = \max(|\mathbf{o}_n|^2) / \text{mean}(|\mathbf{o}_n|^2)$ 
16:   end for
17:   if RIM-RS scheduled in this slot then
18:      $\mathbf{z}_n = \text{concatenate}(\mathbf{z}_n, \mathbf{p})$ 
19:      $N_{\text{RS}} = N_{\text{RS}} + 1$ 
20:   else if RIM-RS not scheduled in this slot then
21:      $\mathbf{w} = \text{concatenate}(\mathbf{w}, \mathbf{p})$ 
22:   end if
23: end for

```

---



---

**Algorithm 2** Threshold determination for Detector 2
 

---

```

1:  $P_f = 0.01$  ▷ False alarm probability target
2:  $u = \text{round} \left( \frac{\text{length}(\mathbf{w})}{1 - P_f} \right)$ 
3:  $\mathbf{w}_{\text{sort}} = \text{sort}(\mathbf{w})$ 
4:  $\gamma = \mathbf{w}_{\text{sort}}(u)$  ▷ Detection threshold
5: for  $n = 1$  to  $N_s$  do
6:    $d_n = \text{length}(\text{find}(\mathbf{z}_n > \gamma))$ 
7:    $P_{d,n} = d_n / N_{\text{RS}}$ 
8: end for
9:  $P_d = \sum_{n=1}^{N_s} P_{d,n} / N_s$  ▷ Detection probability

```

---

### 3.2 Performance metrics

One of the main purposes of the upcoming evaluations is to compare the two RIM-RS designs and define the minimum SNR requirements where the RIM-RS can still be detected under large propagation delays. To this end, the following three metrics are used in the evaluations [10]:

1. *The detection probability ( $P_d$ )* is defined as the probability of detecting a sequence in a detection window given that the sequence is present in that detection window. As there are multiple detection windows within a delay window, if a sequence is detected in multiple adjacent detection windows, it is considered only once for the detection probability. Target value is 90%.
2. *The false alarm probability ( $P_f$ )* is defined based on detecting any of the sequences in a detection window when no sequence was transmitted. Target value is 1%.
3. *The detection error probability ( $P_e$ )* is defined as the probability that the detected sequence does not correspond to the possible set of active sequences actually arriving within the detection window. Target value is 1%.

## 4 Results and discussion on RIM-RS detection performance

All evaluations are performed using a 3GPP 5G NR standardization compliant radio link simulator based on the agreed simulation assumptions for the Release-16 NR-RIM study item [10]. An additive white Gaussian noise (AWGN) channel model with random phase rotation is assumed as a baseline to evaluate the detection performance of different 5G NR RIM-RS transmission schemes [10]. We extend the analysis by including a tapped-delay-line (TDL-E) fading channel model [19], which models a line-of-sight channel with first tap following Ricean distribution with a K-factor of  $K = 22$  dB and a root-mean-squared delay spread of 30 ns. The main link level parameters used in this study are summarized in Table 3.

Focusing on the most realistic scenarios in the NR-RIM framework, the main topic of this study is to comprehensively evaluate the RIM-RS designs with multiple different RIM-RS sequences transmitted from multiple gNBs, corresponding to case C4. First, reference performance results are shown in the upper part of Table 4, following simulation assumptions as depicted in [12]. Then, we evaluate the achievable gain obtained by using the enhanced receiver algorithm, defined as Detector 2, with and without increased number of detection windows and the results are shown in the lower part of Table 4. Next, we evaluate the performance improvement in terms of detection probability for all proposed grouping-based RIM-RS transmission schemes in Table 5. Finally, performance results for a fixed number of simultaneously transmitting gNB are illustrated in Table 6. In all the cases and upcoming numerical results, we target 90% detection probability under the 1% false alarm rate and the 1% detection error rate, as discussed in Sect. 3. For the cases where 90% detection probability is not achieved, the detection probability at -10 dB SNR point is provided.

**Table 4** Detection performance in terms of required SNR in dBs for 90% detection probability, when all RIM-RS sequences are transmitted using the same frequency domain resources and when using Detector 1 [12] (top) or Detector 2 (bottom) with the enhanced receiver algorithm and using different number of detection windows ( $N_w$ ). Here,  $M_C = 10$  is assumed

		AWGN												TDL-E											
Detector 1	$N_S = 1, M_{gNB} = 10$ $N_S = 2, M_{gNB} = 20$ $N_S = 4, M_{gNB} = 40$ $N_S = 8, M_{gNB} = 80$	$1OS\ RS\ (N_w = 5)$				$2OS\ RS\ (N_w = 3)$				$1OS\ RS\ (N_w = 5)$				$2OS\ RS\ (N_w = 3)$											
		comb1	comb2	comb4	comb4	comb1	comb2	comb4	comb4	comb1	comb2	comb4	comb4	comb1	comb2	comb4	comb4								
		-16.2	-15.0	75%	-17.0	-14.6	40%	-17.9	-17.2	-16.1	-18.9	-18.1	-15.7												
		-15.9	-13.8	62%	-16.2	-12.0	16%	-16.5	-15.2	-10.4	-17.2	-15.2	70%												
		-14.5	-9.2	23%	-14.1	58%	3%	-14.7	-10.2	52%	-14.3	75%	22%												
		-9.5	45%	5%	37%	12%	-	-8.2	52%	13%	46%	22%	2%												
Detector 2	$N_S = 1, M_{gNB} = 10$ $N_S = 2, M_{gNB} = 20$ $N_S = 4, M_{gNB} = 40$ $N_S = 8, M_{gNB} = 80$	$1OS\ RS\ (N_w = 5)$				$2OS\ RS\ (N_w = 3)$				$1OS\ RS\ (N_w = 5)$				$2OS\ RS\ (N_w = 3)$											
		-18.1	-17.1	-16.0	-19.2	-17.2	-15.3	-19.3	-18.6	-17.9	-20.6	-19.4	-18.4												
		-17.8	-16.5	-15.2	-19.0	-16.5	-14.4	-18.2	-17.2	-16.2	-19.5	-17.9	-16.2												
		-17.1	-15.4	-13.6	-18.1	-15.2	-12.2	-17.2	-15.6	-14.0	-18.1	-15.6	-13.1												
		-15.2	-12.0	88%	-15.7	-6.0	78%	-14.9	-11.3	89%	-15.2	-2.0	78%												
Detector 2	$N_S = 1, M_{gNB} = 10$ $N_S = 2, M_{gNB} = 20$ $N_S = 4, M_{gNB} = 40$ $N_S = 8, M_{gNB} = 80$	$1OS\ RS\ (N_w = 9)$				$2OS\ RS\ (N_w = 5)$				$1OS\ RS\ (N_w = 9)$				$2OS\ RS\ (N_w = 5)$											
		-18.0	-17.1	-16.0	-19.2	-17.5	-15.9	-19.2	-18.5	-17.8	-20.6	-19.6	-18.6												
		-18.0	-16.7	-15.5	-19.1	-17.2	-15.5	-18.3	-17.4	-16.4	-19.6	-18.2	-17.0												
		-17.6	-16.3	-15.1	-18.6	-16.6	-15.1	-17.7	-16.4	-15.4	-18.7	-16.9	-15.4												
		-17.4	-15.5	-14.4	-17.4	-15.3	-13.9	-17.3	-15.3	-14.3	-17.4	-15.1	-13.8												

**Table 5 Detection performance in terms of required SNR in dBs for 90% detection probability, when using propagation delay based gNB grouping for the proposed schemes A, B, and C. Here,  $M_C = 10$  is assumed**

Detector 2	AWGN								TDL-E							
	1OSRS ( $N_w = 9$ )				2OSRS ( $N_w = 5$ )				1OSRS ( $N_w = 9$ )				2OSRS ( $N_w = 5$ )			
	comb1	comb2	comb4	comb4	comb1	comb2	comb4	comb4	comb1	comb2	comb4	comb4	comb1	comb2	comb4	comb4
<b>Scheme A</b>																
$N_S = 1, M_{gNB} = 10$	-18.7	-18.2	-13.3	-17.8	-20.3	-19.6	-17.8	-17.8	-18.6	-17.8	-14.0	-14.0	-20.1	-19.2	-16.9	-16.9
$N_S = 2, M_{gNB} = 20$	-18.7	-17.5	-14.9	-17.6	-20.1	-18.1	-17.6	-17.6	-18.4	-17.1	-14.9	-14.9	-20.0	-18.1	-17.4	-17.4
$N_S = 4, M_{gNB} = 40$	-18.6	-16.9	-16.1	-16.2	-19.2	-18.0	-16.2	-16.2	-18.4	-16.6	-15.7	-15.7	-19.1	-17.4	-15.9	-15.9
$N_S = 8, M_{gNB} = 80$	-17.5	-16.2	-15.0	-15.7	-18.4	-16.5	-15.7	-15.7	-17.4	-15.9	-14.7	-14.7	-18.2	-16.1	-15.4	-15.4
<b>Scheme B</b>																
$N_S = 1, M_{gNB} = 10$	-18.7	-18.2	-13.3	-17.8	-20.3	-19.6	-17.8	-17.8	-18.6	-17.8	-14.0	-14.0	-20.1	-19.2	-16.9	-16.9
$N_S = 2, M_{gNB} = 20$	-19.1	-17.8	-14.9	-17.4	-19.6	-18.1	-17.4	-17.4	-18.9	-17.2	-14.9	-14.9	-19.5	-17.9	-17.1	-17.1
$N_S = 4, M_{gNB} = 40$	-18.8	-16.9	-15.9	-15.3	-19.2	-17.5	-15.3	-15.3	-18.6	-16.5	-15.3	-15.3	-19.3	-17.2	-15.2	-15.2
$N_S = 8, M_{gNB} = 80$	-17.7	-15.7	-13.3	-13.2	-18.3	-15.5	-13.2	-13.2	-17.5	-15.1	-12.9	-12.9	-18.2	-15.2	-13.0	-13.0
<b>Scheme C</b>																
$N_S = 1, M_{gNB} = 10$	-18.8	-18.1	-13.4	-17.3	-20.1	-17.8	-17.3	-17.3	-18.5	-17.9	-13.9	-13.9	-20.0	-17.5	-16.8	-16.8
$N_S = 2, M_{gNB} = 20$	-18.7	-17.2	-12.9	-13.1	-20.1	-16.2	-13.1	-13.1	-18.5	-17.0	-12.5	-12.5	-20.0	-16.0	-12.8	-12.8
$N_S = 4, M_{gNB} = 40$	-18.6	-16.2	-14.1	-12.8	-19.2	-14.3	-12.8	-12.8	-18.4	-15.8	-13.8	-13.8	-19.0	-13.9	-12.3	-12.3
$N_S = 8, M_{gNB} = 80$	-17.3	-15.1	-12.0	-10.6	-18.4	-13.4	-10.6	-10.6	-17.2	-14.8	-11.7	-11.7	-18.1	-12.9	-9.9	-9.9



**Table 6** Detection performance in terms of required SNR in dBs for 90% detection probability, when using either uniformly distributed gNB delays as in [12] or propagation delay based gNB grouping for the proposed scheme A. Here, a fixed number of simultaneously transmitting gNBs,  $M_{\text{gNB}} = 80$ , is assumed

Detector 2	AWGN				TDL-E												
	10S RS ( $N_w = 9$ )				20S RS ( $N_w = 5$ )				10S RS ( $N_w = 9$ )				20S RS ( $N_w = 5$ )				
	comb1	comb2	comb4	comb4	comb1	comb2	comb4	comb4	comb1	comb2	comb4	comb1	comb2	comb4	comb1	comb2	comb4
<b>w/o grouping</b>																	
$M_C = 80, N_S = 1$	-33.4	-29.7	-26.1	-24.2	-35.1	-28.1	-24.2	-24.2	-32.8	-29.0	-26.3	-34.3	-27.3	-23.6			
$M_C = 40, N_S = 2$	-19.6	-18.4	-17.7	-17.6	-20.2	-18.3	-17.6	-17.6	-21.6	-20.5	-19.8	-22.4	-21.0	-20.0			
$M_C = 20, N_S = 4$	-18.4	-17.1	-16.6	-16.0	-18.3	-16.1	-16.0	-16.0	-18.9	-17.6	-17.1	-19.1	-17.1	-16.7			
$M_C = 10, N_S = 8$	-17.4	-15.5	-14.4	-13.9	-17.4	-15.3	-13.9	-13.9	-17.3	-15.3	-14.3	-17.4	-15.1	-13.8			
<b>Scheme A</b>																	
$M_C = 80, N_S = 1$	-33.2	-29.9	-26.6	-23.0	-33.7	-26.4	-23.0	-23.0	-32.1	-29.1	-25.7	-32.8	-25.8	-22.5			
$M_C = 40, N_S = 2$	-21.2	-21.6	-20.7	-21.4	-23.3	-23.1	-21.4	-21.4	-20.9	-21.7	-20.6	-22.9	-22.6	-21.2			
$M_C = 20, N_S = 4$	-19.8	-19.1	-18.5	-19.2	-20.7	-19.4	-19.2	-19.2	-19.0	-18.2	-18.3	-20.1	-19.1	-18.5			
$M_C = 10, N_S = 8$	-17.5	-16.2	-15.0	-15.7	-18.4	-16.5	-15.7	-15.7	-17.4	-15.9	-14.7	-18.2	-16.1	-15.4			

#### 4.1 Receiver detection algorithm enhancements

The detection probability results are presented in the upper part of Table 4 in line with earlier results in [12]. These results highlight that the 1OS design outperforms the 2OS design in the more challenging scenarios with up to 40 or 80 gNBs transmitting a RIM-RS sequence. In the specific case of  $M_{\text{gNB}} = 80$  and AWGN channel, the 2OS RIM-RS design is not able to achieve the 90% detection probability target value even with the comb-1 pattern.

The detection performance results obtained using the new detector threshold definition based on the knowledge of the receiver noise correlation statistics are summarized in the middle part of Table 4. It should be noted that in this case, all RIM-RS sequences are transmitted using the same frequency domain resources from gNBs uniformly located within a given propagation delay range, similarly to [12]. In general, significant performance improvement is achieved with a sequence detector optimizing the false alarm probability. In addition, all evaluated cases are able to achieve the detection probability target for comb-1 and comb-2 patterns, opening up the possibility of using frequency-division multiplexing schemes with comb-2 layouts. The 1OS design provides better performance compared to the 2OS design when using comb-2 and comb-4 structures as highlighted for the results obtained using Detector 1, when using five and three detection windows for 1OS and 2OS RIM-RS design, respectively. The 1OS design could be more suitable for remote interference detection in the most realistic scenarios with larger number of base stations deployed, i.e, 40 and 80 gNBs, and with four or eight sequences used in the network. This relates to the higher interference and overlap between sequences with the 2OS RIM-RS due to its longer time duration [12]. These results motivate the analysis of the maximum achievable performance using a fixed number of simultaneously transmitting gNBs in practical scenarios, i.e, 80 gNBs, using different number of sequences  $N_S$  in the network, as will be discussed in Sect. 4.3.

Performance results for the enhanced receiver algorithm with increased number of detection windows are shown in the lower part of Table 4. Intuitively, increasing further the number of detection windows from five to nine for the 1OS RIM-RS design and from three to five for the 2OS RIM-RS design provides higher probability to capture maximum amount of received energy of the transmitted sequence within a single detection window. In addition, even though the received RIM-RS is not perfectly aligned to a specific detection window, using more detection windows increases the probability to detect the signal under varying interference conditions. In comparison to the performance results evaluated for lower number of detection windows, up to 3 dB gain can be achieved when 40 gNBs are transmitting simultaneously. Especially, for the 2OS design, increasing the number of the detection windows improves the performance with comb-2 and comb-4 when  $M_{\text{gNB}} = 80$ . For the case of 80 gNBs, the 90% detection probability target value can be achieved in all cases and with both RIM-RS designs, highlighting the potential use of frequency multiplexing between gNBs or gNB groups. In addition, with increased number of detection windows, the performance of 1OS and 2OS RIM-RS designs is quite similar in different scenarios.

In general, distances in the range of 64 to 400 km between aggressor and victim gNBs groups can be assumed based on trial results from TD-LTE networks [10], where the largest contribution to the interference was due to the base stations within a distance

of 150 km. In general, based on [3], the pathloss can be smaller than the free space path loss in the case of atmospheric ducting phenomenon. Aiming to provide a conservative estimate of the SNR required to detect the remote interference we use Friis transmission equation [20] for pathloss modeling assuming 3.5 GHz carrier frequency, -101 dBm noise power for the active band used by RIM-RS, and a typical base station transmission power of +43 dBm. In that context, the SNR requirements to detect the remote interference corresponds to approximately -2.5 and -11 dB for 150 and 400 km, respectively. Therefore, these results highlight that the improved detection algorithm assures that both RIM-RS designs can provide sufficient performance to detect the remote interference under the atmospheric ducting phenomenon in all cases described in Table 1. Nevertheless, the good performance achieved using comb-2 or comb-4 structure with the 1OS design allows the RIM-RS to be frequency multiplexed with other DL transmissions among gNBs within the region of the gNB group. The 2OS RIM-RS design breaks the symbol alignment of the 5G NR physical layer and thus does not allow to multiplex DL transmissions. Based on these results, the enhanced receiver algorithm is assumed and deployed in all the upcoming evaluations.

#### 4.2 Propagation delay based gNB grouping transmissions

The performance obtained when grouping several gNBs located in the same area into sets of  $M_G = 10$ , as illustrated in Fig. 2, is shown in Table 5 for the considered schemes A, B, and C. The most significant gain in performance is obtained for the case of four or eight base sequences used in the network compared to the results shown in Table 4 without grouping. When larger number of gNBs are deployed in practical RIM scenarios, such as 40 or 80 gNBs, the benefit of grouping them according to the base sequence transmitted improves the receiver detection processing assuming different transmission time for each group, especially with 2OS RIM-RS design. On the other hand, there is no benefit on using grouping-based RIM-RS transmission schemes in scenarios with 20 gNBs or less deployed, and when just one or two base sequences are used in the network.

Focusing mainly on the most practical RIM scenarios with more than 20 gNBs located on an area affected by ducting phenomenon, better results are systematically obtained using schemes A and B, when the different base sequences are multiplexed using same CS per sequence, compared to scheme C, where different CSs are used to transmit the same sequence from different gNBs. The separation capability to distinguish between transmitted RIM-RS sequences is related to the auto- and cross-correlation properties of the selected sequences. It should be noted that when the received sequence is not fully located within the detection window, the correlation between the received RIM-RS and the local reference is deteriorated leading to high error detection probability. Hence, due to the lower number of copies per sequence allocated within a specific CS in scheme C for comb-2 and comb-4 structures, the achievable detection performance is degraded.

The detection performance improvement attained by schemes A and B in the NR-RIM framework suggest their suitability to take them as baseline for grouping-based RIM-RS transmissions. All evaluated cases assure the detection of the remote interference for both RIM-RS designs based on the SNR requirements described in Sect. 4.1. Therefore, in the case of transmission scheme B, the 1OS design could be used to allow UEs within

the transmitting gNB group to perform interference channel measurements by using the scheduled RIM-RS as ZP and NZP CSI-RS. Nevertheless, in the specific case of eight different sequences and eight aggressor gNB groups in the network, results obtained by using transmission scheme A achieve better performance. In addition, this scheme can be used to differentiate aggressor gNB groups by the transmitted sequence leading to the possibility of applying corresponding RIM mitigation schemes directly based on detected sequence.

#### 4.3 Fixed number of simultaneously transmitting gNBs

As a final example, we focus on a fixed number of simultaneously transmitting gNBs and on the comparison of the achievable gain obtained with transmission scheme A against uniformly distributed gNB delays. The detection performance results shown in Table 6, analyze the maximum achievable performance within the NR-RIM framework when the total number of gNBs transmitting a RIM-RS sequence is fixed to  $M_{\text{gNB}} = 80$ , and with varying number of base sequences used in the network. Based on the presented evaluations, at least 80 gNBs sharing the same base sequence can be supported while ensuring high detection probability with the assumed enhanced receiver algorithms. This indicates that relatively large gNB groups can be supported in practical scenarios to improve detection reliability. In comparison to results shown in Table 4, increasing the number of transmitted copies per base sequence considerably improves the detection performance.

The gNB grouping based on scheme A allows to clearly improve the detection performance when multiple base sequences are transmitted in the network. As without grouping, the lowest detection SNR is achieved when all gNBs are transmitting the RIM-RS using the same base sequence. These results also indicate that with multiple base sequences the group size could be increased further with scheme A to improve the detection performance. The most important feature of gNB grouping based on the presented scheme A is that it allows to identify different groups based on the detected base sequence with high probability when using the presented enhanced detector. This is not possible in the non-grouping based approach, in which no clear structure is given to gNBs to enable adaptive RIM solutions.

This feature of scheme A is of particular significance considering that the atmospheric ducting phenomenon is typically affecting relatively large regions simultaneously and the need of coordination between operators, possibly operating in different countries, can be expected in the NR-RIM framework. Therefore, grouping gNBs deployed per operator following the scheme A can help to apply adaptive RIM mitigation schemes between different operators, possibly even in different countries.

## 5 Conclusion

In this article, the remote radio interference stemming from atmospheric ducting phenomenon was studied, with particular emphasis on 5G NR networks. Two alternative reference signal structures for remote interference detection were described, together with the corresponding receiver processing framework and algorithms. In addition, three feasible propagation delay based gNB grouping schemes were presented and evaluated in the NR-RIM framework, together with enhanced receiver algorithms, targeting to improve the detection performance with large number of gNBs and base sequences.

The obtained detection performance results show that in practical 5G NR deployment scenarios, the performance of 1OS and 2OS RIM-RS designs are approximately on the same level. The overhead of the 1OS RIM-RS design is smaller and allows to be frequency multiplexed with other DL transmissions, e.g., allowing to use them for NR CSI measurements for UEs served by the gNBs in the gNB group transmitting the RIM-RS, when comb-2 or comb-4 structure is used. The formulated improved detection algorithm with fixed false alarm rate and increased number of detection windows assures that both RIM-RS designs can detect the remote interference under the atmospheric ducting phenomena for all evaluation cases described in the latest 3GPP specifications for NR-RIM.

Overall, propagation delay based gNB grouping using the presented scheme A provides the best detection performance among all grouping-based transmission schemes with up to 80 simultaneously transmitting gNBs. On the other hand, frequency multiplexing the different base sequences using scheme B provides better detection performance results than frequency multiplexing the same base sequence over different frequency resources using scheme C. In this case, the lower number of copies of transmitted sequences with a specific cyclic shift degrades the achievable detection performance. Hence, schemes A and B can be considered as potential candidates for grouping-based RIM-RS transmissions due to the improved detection performance. The proposed scheme B provides improved possibilities for UE interference measurements, but does not support base sequence based gNB group identification. For the proposed scheme A, victim or aggressor gNB groups can be differentiated by the transmitted base sequence, leading to the possibility of applying adaptive RIM mitigation schemes.

#### Abbreviations

3GPP: 3rd generation partnership project; 5G NR: Fifth generation new radio; AWGN: Additive white Gaussian noise; BS: Base station; CP: Cyclic prefix; CS: Cyclic shift; CSI-RS: Channel state information reference signal; DL: Downlink; DM-RS: Demodulation reference signal; GP: Guard period; LTE: Long term evolution; N-ZP: Non-zero power; OAM: Operations, administration and maintenance; OFDM: Orthogonal frequency division multiplexing; OS: OFDM symbol; PRACH: Physical random access channel; PSS: Primary synchronization signal; RIM: Remote interference management; RS: Reference signal; SCS: SubCarrier spacing; SNR: Signal to noise ratio; SSS: Secondary synchronization signal; TDD: Time division duplexing; TDL: Tapped delay line; UE: User equipment; UL: Uplink; ZP: Zero power.

#### Acknowledgements

The work was supported in part by the Finnish Funding Agency for Innovation (Business Finland), under the project 5G-FORCE.

#### Authors' contributions

EP is the main author of the study and carried out the experimental work. TL contributed to the development of the ideas, result analysis, and article writing. MM, YY, KP, SN, and MV reviewed and edited the manuscript. All authors conceived and designed the study, and read and approved the manuscript.

#### Funding

They are presented in the "Acknowledgements" section.

#### Availability of data and materials

Data sharing not applicable to this article as no datasets were generated or analysed during the current study.

#### Competing interests

The authors declare that they have no competing interests.

#### Author details

<sup>1</sup> Nokia Bell Labs, Tampere, Finland. <sup>2</sup> Nokia Bell Labs, Espoo, Finland. <sup>3</sup> Wireless System Engineering Finland Ltd., Tampere, Finland. <sup>4</sup> Nokia Bell Labs, Seoul, Republic of Korea. <sup>5</sup> Nokia Bell Labs, Aalborg, Denmark. <sup>6</sup> Department of Electrical Engineering, Tampere University, Tampere, Finland.

Received: 23 December 2019 Accepted: 9 February 2021

Published online: 05 March 2021

## References

1. M. Shafi, A.F. Molisch, P.J. Smith, T. Haustein, P. Zhu, P. De Silva, G. Wunder, 5G: a tutorial overview of standards, trials, challenges, deployment, and practice. *IEEE J. Sel. Areas Commun.* **35**(6), 1201–1221 (2017)
2. E. Dahlman, S. Parkvall, J. Skold, *5G NR: The Next Generation Wireless Access Technology* (Academic Press, Cambridge, 2018).
3. E. Dinc, O.B. Akan, Channel model for the surface ducts: large-scale path-loss, delay spread, and AOA. *IEEE Trans. Antennas Propag.* **63**(6), 2728–2738 (2015)
4. J.D. Turton, D.A. Bennetts, S.F.G. Farmer, An introduction to radio ducting. *Meteorol. Mag.* **117**(1393), 245–254 (1988)
5. Q. Liao, Z. Sheng, H. Shi, J. Xiang, H. Yu, Estimation of surface duct using ground-based GPS phase delay and propagation loss. *Remote Sensing* **10**(5), 724 (2018)
6. S. Mentés, Z. Kaymaz, Investigation of surface duct conditions over Istanbul, Turkey. *J. Appl. Meteorol. Clim.* **46**(3), 318–337 (2007)
7. T. Zhou, T. Sun, H. Hu, H. Xu, Y. Yang, I. Harjula, Y. Koucheryavy, Analysis and prediction of 100 km-scale atmospheric duct interference in TD-LTE networks. *J. Commun. Inf. Netw.* **2**(1), 66–80 (2011)
8. Y. Wang, Y. Chen, T. Zhou, H. Hu, A traceable approach to remote interference management for new radio, in *International Conference on Communications Workshops (ICC Workshops)*. (IEEE, 2019), pp. 1–6
9. H.K. Son, H.J. Hong, Interference analysis through ducting on Korea's LTE-TDD system from Japan's WiMAX, in *International Conference on Information and Communication Technology Convergence (ICTC)*. (IEEE, 2014), pp. 802–805
10. Technical Specification Group Radio Access Network. Study on remote interference management for NR (Release 16), document TR 38866 V16.1.0, 3GPP, March (2019)
11. A. Shen, Y. Zhang, B. Guo, G. Wang, Y. Gao, Liu, J., T. Xie, Monitoring and avoidance of atmospheric duct on interference optimization in TD-LTE system, in *International Conference Signal And Information Processing, Networking & Computers* (2017), pp. 36–45
12. E. Peralta, M. Mäenpää, T. Levanen, Y. Yuk, K. Pedersen, S. Nielsen, M. Valkama, Reference signal design for remote interference management in 5G new radio, in *European Conference on Networks and Communications (EuCNC)* (IEEE, 2019), pp. 559–564
13. S. Shim, Y.A.N.G. Hayoung, J. Lee, H.A. Kilsik, *Method and Apparatus for Controlling Interference due to Atmospheric Ducting in Wireless Communications System*, U.S. Patent Application No. 15/929,530 (2020)
14. D.J. Ryan, R. Menon, J. Yun, E. Gormley, *Detecting Tropospheric Ducting Interference in Cellular Networks*, U.S. Patent Application No. 16/503,319 (2020)
15. Technical Specification Group Radio Access Network. Physical channels and modulation (Release 16), document TR 38211 V16.3.0, 3GPP, September (2020)
16. Technical Specification Group Radio Access Network. Physical channels and modulation (Release 16), document TR 36211 V16.3.0, 3GPP, September (2020)
17. R. Gold et al., Optimal binary sequences for spread spectrum multiplexing. *IEEE Trans. Inf. Theory* **13**(4), 619–621 (1967)
18. Tchebichef, P.: Des valeurs moyennes. *Journal de Mathématiques Pures et Appliquées* **2**(12), 177–184 (1867)
19. Technical Specification Group Radio Access Network. Study on channel model for frequencies from 0.5 to 100 GHz (Release 16), document TR 38901 V16.1.0, 3GPP, December (2019)
20. H.T. Friis, A note on a simple transmission formula. *Proc. IRE* **34**(5), 254–256 (1946)

## Publisher's Note

Springer Nature remains neutral with regard to jurisdictional claims in published maps and institutional affiliations.

Submit your manuscript to a SpringerOpen<sup>®</sup> journal and benefit from:

- Convenient online submission
- Rigorous peer review
- Open access: articles freely available online
- High visibility within the field
- Retaining the copyright to your article

---

Submit your next manuscript at ► [springeropen.com](https://www.springeropen.com)

---